J. Phys. D: Appl. Phys.

Revised

7 October 2014

Switching and Memory Characteristics of Thin Films of an Ambipolar Organic Compound: Effects of Device Processing and Electrode Materials

Myung-Won Lee,[a)] Christopher Pearson, Tae Jung Moon,[b)] Alison L Fisher and Michael C Petty[c)]

School of Engineering and Computing Sciences, and Centre for Molecular and Nanoscale Electronics, Durham University, Durham, DH1 3LE, United Kingdom

[a)]Current address: System LSI Division, Samsung Electronics Co. LTD., Yongin-City Gyeonggi-do, 446-711, Korea.

[b)]Current address: Subdivision of Electronic Information Engineering, Kyungnam College of Information & Technology, 45, Jurye-ro, Sasang-gu, Busan, 617-701, Korea.

[c)]To whom correspondence should be addressed: phone: +44 (0) 191 334 2419; Fax: +44 (0) 191 334 2407; e-mail: m.c.petty@durham.ac.uk

Abstract

We report on the effects of device processing conditions, and of changing the electrode materials, on the switching and negative differential resistance (NDR) behaviour of metal/organic thin film/metal structures. The organic material was an ambipolar molecule containing both electron transporting (oxadiazole) and hole transporting (carbazole) chemical groups. Switching and NDR effects are observed for device architectures with both electrodes consisting of aluminium; optimized switching behaviour is achieved for structures incorporating gold nanoparticles. If one of the Al electrodes is replaced by a higher work function metal or coated with an electron-blocking layer, switching and NDR are no longer observed. The results are consistent with a model based on the creation and destruction of Al filaments within the thin organic layer.

KEYWORDS: *Electronic memory devices, organic thin film switches, negative differential resistance.*

1. Introduction

The past decade has seen an upsurge in academic and commercial interest in the field of organic electronics [1-4]. Devices such as organic light emitting displays, and chemical and physical sensors are already in the marketplace, while others, including field effect transistors, photovoltaic cells and smart cards, are developing fast. In order for organic electronics to realise its full potential, it is essential that a further basic circuit element is developed – a memory cell. Although memories represent by far the largest part of conventional (silicon-based) electronic systems, work on organic memories is lagging significantly behind the development of organic transistors. Many different concepts have been proposed, but there is currently no consensus on the way forward [5-10].

The intense activity in the study of resistive memory technologies is motivated by their very simple structure and ability for scaling to small dimensions [11-15]. Such devices can be stacked in multiple levels, providing 3-d architectures [16]. Flexible and moldable memory structures have also been reported [17]. Organic resistive memories are generally formed by interposing thin layers of organic molecules between two electrodes. The cross-point (or crossed-bar) device permits the closest packing of bit-cells, with each occupying an area of $4F^2$, where F is the minimum feature size (the line-width and spacing of the electrodes). A very wide range of organic materials that exhibit resistive switching has now been reported [10]. The film thicknesses are generally less than 1 μm and the switching phenomena are also observed in other types of material (e.g. inorganic compounds such as silicon dioxide and metal oxides). Furthermore, the thin films have been formed using a variety of techniques (e.g. spin-coating, thermal evaporation). The only experimental parameter that is common to all the structures studied is the presence of metallic electrodes (e.g. Al) below and on top of the thin film.

Despite the impressive progress on developing the technology (e.g. 3-d structures), there is no agreement on how resistive thin film memories operate. Explanations have generally fallen into two distinct categories: (i) the injection and storage of charge in the thin film; and (ii) metallic filament formation. There is increasing evidence that filamentary conduction plays an important role in the

memory operation and can account for much of the experimental data in the literature. In previous work, we have reported on bistable switching phenomena in Al/thin film/Al structures in which the thin film is an ambipolar electroactive organic compound containing both electron and hole transporting groups [18-20]. Here, we explore the effects of device processing and of varying the electrode materials. The results support the view that the formation and destruction of metallic filaments within the organic thin film can account for both switching and negative differential resistance (NDR) in these devices.

2. Experimental details

The organic compound used in this study was 2-(4-(7-(9*H*-carbazol-9-yl)-9,9-dihexyl-9*H*-fluoren-2-yl)phenyl)-5-(4-*tert*-butylphenyl)-1,3,4-oxadiazole; the material was synthesized as described previously and has been used in the fabrication of organic light-emitting devices [21]. This compound is an ambipolar molecule, incorporating both electron transporting (oxadiazole) and hole transporting (carbazole) chemical groups. The generic device architecture investigated in this work is provided in Figure 1(a). A photograph of the fabricated device array is shown in Fig. 1(b) while the molecular structure of the ambipolar molecule is depicted in Fig. 1(c). Devices were all prepared in a Class 1,000 microelectronics clean room. The substrates were generally glass microscope slides; these were scrupulously cleaned using the procedure described previously [18].

In this work, the top electrode material was thermally evaporated aluminium, while a systematic investigation into changing the bottom electrode was undertaken. Reference devices were made by using bottom electrodes consisting of 100 nm thick strips of aluminium, in most cases 380 μm wide and 1024 μm apart; some data (noted in the text) were obtained using electrode strips 1.5 mm wide and 1.5 mm apart. The aluminium electrodes were deposited by thermal evaporation through a shadow mask at a rate of 0.5±0.1 nm s^{-1} under a vacuum of approximately $5x10^{-6}$ mbar. For certain devices, the metallized substrates were spin coated with a 40–45 nm thick layer of poly(3,4-ethylenedioxythiophene)-poly(styrenesulfonate) from aqueous dispersion (PEDOT-PSS; CLEVIOS P VP AI 4083, Heraeus, Germany). Before coating, 3 ml of the PEDOT-PSS solution was passed

through a 0.2 μm syringe filter to remove any residual particulates. Then, 200 μl of the filtered dispersion was applied to the surface of the substrate, which was spun at 2500 rpm for 45 s. The PEDOT-PSS coated substrates were annealed at 180 °C for 2 minutes to remove any residual water.

The ITO was patterned into the same 1.5 mm wide strips as used for some of the Al bottom electrodes using a resist pen. Other devices were fabricated on glass slides coated with evaporated gold; a thin layer of Cr (~10 nm) was first thermally evaporated through a shadow mask (to produce the strip pattern) followed by approximately 100 nm of Au. The rates of evaporation for both metals was 0.1 ± 0.02 nm s^{-1}.

A solution of the ambipolar compound was prepared by adding 1 ml of Fisher Chemical Trace Analysis Grade chloroform to the solid to give a concentration of 6.70 g l^{-1}. The active organic layer was deposited by spin-coating 150 μl of this solution onto the bottom electrode, unless stipulated otherwise at 700 rpm, for 50 s in a glove-box under a nitrogen atmosphere. Organically capped nanoparticles (NPs) used in this work were prepared and incorporated into the organic films as described previously [18]. The gold nanoparticles (Q-Au) were of nominal diameter 10 nm passivated with tri-*n*-octylphosphine oxide/octadecylamine. For devices containing the nanoparticles, 0.17 ml of a 0.2 g l^{-1} chloroform solution of NPs was added to the ambipolar solution, to give a solution of 0.5 wt % of nanoparticles. The spin casting parameters for NP-doped films were the same as those for the pure material.

To complete the devices, 100 nm thick aluminium strips perpendicular to and having the same dimensions as the bottom electrodes, were thermally evaporated on top of the organic layers. The evaporation conditions were the same as those used for the bottom electrodes. In the case of CsF-modified top electrodes, caesium fluoride (Aldrich, 99.00%) was thermally evaporated though a shadow mask to give the required film thickness; the evaporation rate was of 0.05 ± 0.01 nm s^{-1}.

The thicknesses of the organic layers were measured by mechanically removing the film (by abrasion in an area between the metal electrodes) and then imaging the step created using a Digital Instruments NanoMan II AFM in tapping mode. The surface roughnesses (roughness average - R_a

parameter) were measured with the same AFM. Electrical characterization of the devices was undertaken with the samples in vacuum and using a Keithley 2400 Sourcemeter.

3. Results and discussion

3.1 Device Processing

As noted by ourselves and other workers, a positive voltage had to be applied to the top Al electrode before any switching effects were observed. This process is referred to as device 'formation.' In our work, an increasing positive voltage scan starting at 0 V was applied to new devices until switching and negative differential resistance (NDR) were observed; the maximum voltage applied was 10 V. The influence of different processing parameters, such as organic layer thickness, post-deposition annealing and the incorporation of metallic nanoparticles within the organic layer, was initially studied. Figure 2 shows the effects of different thickness of the organic layer on the current versus voltage behaviour of the devices following the device formation procedure. The film thickness was varied by changing the spinning speed during the deposition of the ambipolar compound; the thicknesses and surface roughnesses of the three devices depicted in Fig. 2 are provided in Table 1. As expected, higher spin speeds resulted in thinner films, but there is little change in the surface roughness parameter.

The current versus voltage behaviour of the devices shown in Fig. 2 is typical for the device architecture in which the ambipolar organic compound was sandwiched between Al electrodes. These results were obtained using 1.5 mm wide electrodes. Starting with zero applied voltage, the devices are in a low conductivity OFF state. As the applied voltage is increased, the devices switch to a higher conductivity ON state at 2.3 – 3.5 V; higher switching voltages are obtained with thicker films. On further increase in voltage, the currents in the devices become relatively noisy and the NDR regime is entered. A current minimum is achieved between 6 and 9 V; again, this voltage is higher for the thicker films. If the applied voltage is then reduced, the NDR region is followed and the device returns to zero voltage in the ON state, which is retained for subsequent voltage cycling. The devices

could also be reversibly switched between high and low conductivity states. The ON state is obtained by applying a voltage close to the current maximum (i.e. on the low voltage side of the NDR region) and reducing this rapidly to zero (Write process). In contrast, switching from the ON state to the OFF state is accomplished by selecting a voltage corresponding to the current minimum in the NDR region and reducing this rapidly to zero (Erase process). The state of the device (ON or OFF) could be determined by measuring the current at a low voltage, e.g. 1 V (Read process). We have previously suggested that these electrical characteristics are the result of the formation and destruction of metallic filaments in the organic layer [20]. This idea is explored in more detail later in Section 3.4.

All current versus voltage behaviour of the three devices depicted in Fig. 2 are qualitatively similar but differ in detail. The thinnest film (spun at 1000 rpm, Table 1) reveals a low value of the ON/OFF ratio. The voltage required to switch the device from the OFF to the ON state appears to increase with the film thickness; from about 2.2 V for the film spun at 1000 rpm (~50 nm) to about 3.6 V for the film spun at 500 rpm (~100 nm). This suggests that the physical process responsible for switching probably depends on the electric field in the organic thin film. The relationship between current and voltage in both the ON and OFF states of the formed devices can be described by a power law of the form $I \propto V^n$, with $n \sim 1.3$, similar to results reported previously [18]. However, it should be noted that unformed architectures generally show a different current versus voltage dependence – $\log(I/V) \propto V^{1/2}$, typical of Poole-Frenkel conductivity.

Improved ON/OFF switching ratios and less noisy NDR regions were invariably achieved if metallic nanoparticles were mixed in the organic layer prior to spin coating. Earlier work suggested that the incorporation of metallic nanoparticles or nanoclusters was essential before switching and NDR behaviour could be observed [22, 23]. However, it is now evident that switching and NDR can be observed in thin films that do not contain NPs [10]. Figure 3 shows typical current versus voltage characteristics observed with a nanoparticle-containing organic film. Two sets of characteristics are shown (indicated by the two different sets of symbols), measured consecutively, both following the application of a voltage pulse with an amplitude close to the voltage minimum in the NDR region (8

V) to set the device in its OFF state. The electrical characteristics are significantly less noisy than those shown in Fig. 2. The inset shows the same electrical data, but plotted on a log-log scale. Between 0.1 and 1 V, the current versus voltage dependence for the OFF state has the form $I \propto V^{1.27}$, whereas that for the ON state can be described by $I \propto V^{1.26}$. These results are very similar to those described earlier, for devices not containing NPs.

The effect of annealing the organic layer (before evaporation of the top contact, and both with and without the nanoparticles) following spin coating at 700 rpm was also explored. This annealing was performed on a hot plate, in air, at 60 °C for 30 min. The results are summarized in Table 2. It is evident that the post deposition annealing of the organic layer does not improve the ON/OFF ratio. As Table 1 reveals, the annealing process results in a significant reduction in the thickness of the ambipolar film. This will increase the current in the OFF state, probably accounting for the poorer ON/OFF ratios (evident in Fig. 2 for films spin-coated at faster speeds). However, other factors might be important here, including a change in the density and/or morphology of the organic film with annealing.

Other variations in the memory device processing conditions were also explored, including evaporating (instead of spin-coating) the ambipolar organic compound [21] or treating the bottom Al electrode with an oxygen plasma prior to coating with the organic film. The results of these studies remain inconclusive. All the devices worked (i.e. exhibited switching and NDR effects), but with varying success and reproducibility. The 'best' memory devices, in terms of noise-free electrical characteristics, low OFF current, high ON/OFF ratios and clear NDR regions were achieved using organic films of approximately 70 nm in thickness containing 0.5 wt. % Au nanoparticles and not subjecting the devices to thermal annealing.

3.2 Influence of Bottom Electrode Material

In Figure 4(a), the effect of coating the bottom Al electrode with a thin layer (40–45 nm) of PEDOT:PSS is shown. The data presented here are for devices with and without NPs. In both cases, and for both polarities of applied voltage, switching and NDR effects are no longer evident. We have reported on this phenomenon before [20]. The current versus voltage curves shown in Fig. 4(a) are symmetric with regard to the polarity of the applied bias and suggest a bulk-controlled rather than a surface-controlled conductivity process. Attempts were made to fit the electrical data to a number of electrical conduction theories, including space-charge limited conductivity, quantum mechanical tunneling and Schottky emission [24]. The best fits to the experimental data were found using the model for Poole-Frenkel conductivity. This current versus voltage behaviour is related to the reduction of the potential barrier to carriers associated with impurity centres within the material, with the following dependence of current upon voltage

$$I \propto V \exp\left(bV^{1/2}\right) \tag{1}$$

where b is a constant (the Poole-Frenkel constant) given by

$$b = \frac{1}{kT}\left(\frac{e^3}{d\pi\varepsilon_r\varepsilon_0}\right)^{1/2} \tag{2}$$

where d is the film thickness, T is the temperature, k is Boltzmann's constant, ε_0 is the permittivity of free space and ε_r is the relative permittivity of the organic film. We have previously noted that Poole-Frenkel conduction provides a good explanation for the electrical conduction process in unformed resistive memory devices based on a similar compound to that used in this work [18].

The electrical data are shown in Figure 4(b) in the form of log (I/V) versus $V^{1/2}$. These reveal reasonable linearity, over several orders of magnitude of the ordinate variable. Permittivity values for the organic film derived from the slope of the best linear fit (Eqn. (2)) are 35 for the structure without NPs and 17 for the nanoparticle-containing device. These figures are significantly higher than expected. Moreover, the addition of the metallic nanoparticles is expected to increase rather than decrease the permittivity.

The most common form of the Poole-Frenkel equation given by Eqn. (1) is derived from a particular set of equilibrium statistics for the material at zero field. The Poole-Frenkel constant will vary according to the position of the Fermi level. For example, if the material contains donor centres that lie below the Fermi level (and can therefore be regarded as neutral traps, or deep donors) then the Poole-Frenkel constant given by Eqn. (2) will be reduced by a factor of two [24]. In this case, the permittivity values calculated from Fig. 4(b) become: 8.8 (no NPs) and 4.3 (NPs). These values are more in-line with those expected from organic compounds. However, there remains the anomaly of the permittivity of the nanoparticle-containing thin film being less than that of the material with no NPs. As Hill notes [25] the Poole-Frenkel effect given by Eqn. (1) is a limiting case of a more general analysis: carriers can be thermally activated from trapping sites (the basis of Eqn. (1)) or these can tunnel directly to a conduction band (or may undergo a combination of both); the interaction of multiple trapping centres also needs to be taken into account. The nature and distribution of the traps in our organic material will be complex and is likely to be effected by the addition of the nanoparticles. A full understanding of these phenomena must therefore remain the subject of further study.

The effect of using indium-tin-oxide as a bottom electrode is shown in Figure 5(a). Although switching and NDR effects are observed when the top Al electrode is positively biased, these phenomena are no longer observed when the top electrode is biased negatively. In this case, the measured current is relatively high and, as evident in Figure 5(b), shows an almost linear dependence on the applied voltage for voltages up to 10 V. The effect of incorporating a PEDOT:PSS layer between the ITO and the organic film was to suppress the switching and NDR behaviour for both polarities of applied voltage (data not shown). Suppression of the switching and NDR also resulted from the use of an evaporated gold film as the bottom electrode, Figure 6. The current versus voltage behaviour, shown inset as log(I) versus log(V) plots, reveals Ohmic behaviour up to applied voltages of about 7 V.

3.3 Device Top Electrode

Experiments with modifications to the top electrode material were also undertaken. Figure 7 shows the effect of the incorporation of a layer of CsF (produced by vacuum sublimation) beneath the top Al electrode. Relevant device characteristics taken from these (and other) devices are shown in Table 3. It is apparent (Fig. 7) that the additional layer does not affect the ability of the device to switch or to exhibit NDR. For thin CsF layers, the current is increased over that measured for a structure without this additional layer, providing enhanced ON/OFF ratios. However, beyond a CsF thickness of 1.5 nm, the currents decrease. As the CsF layer thickness increases, there is a decrease in the voltage needed to turn the device ON. Moreover, the electrical characteristics appear to be less noisy than those for the structure that does not have the additional CsF layer. The current versus voltage curves for the devices incorporating CsF were symmetrical for different polarities of the applied voltage. In all these respects, the CsF architectures are similar to those incorporating the metallic nanoparticles (Fig. 3).

3.4 Filamentary Conduction Model

Table 4 summarizes the results of our experiments with varying the electrode materials. The data reveal the important influences of both metallic electrodes on the operation of metal/organic thin film/metal structures. First, in all the devices studied, when switching and NDR effects are seen, these phenomena are observed together; this contrasts to some reports in the literature where switching (from a low conductivity state to a state of higher conductivity) is observed without NDR [26-28]. The addition of metallic nanoparticles to the organic thin films results in devices with improved switching characteristics and that are more reproducible. However, the NPs do not appear to alter the

basic operation of the devices or to influence the nature of the conductivity processes in both the ON and OFF states; i.e. the dependences of current on applied voltage for the NP-containing devices shown in Fig. 3 are similar to those shown in Fig. 2 for structures that do not contain nanoparticles.

We suggest that the formation and growth of metal filaments in the organic layer can explain the electrical characteristics of our devices. Figure 8 shows the essential features of a simple model. This is similar to that suggested by Cho et al. [29], which was used to explain the switching in thin film structures with an Ag electrode. During film formation, aluminium ions, formed by oxidation, are injected from the top, positively biased, electrode, drift through the organic film and are subsequently reduced at the bottom electrode to form aluminium, which grows in the form of filaments into the film. When these reach the top electrode, the device switches into a higher conductivity regime. In a previous publication, we have provided electron microscopy evidence for such filaments [20].

We consider that the creation of a network of conductive filaments throughout the organic film constitutes the device formation. The reason that a positive voltage applied to the top electrode is needed for device formation is that the associated oxide layer beneath the top Al electrode will be thinner than that on the bottom electrode, allowing easier filament formation. Following formation, the application of an increased voltage results in excessive heat dissipation within these filamentary regions, leading to their destruction. This explains the (relatively noisy) NDR region. However, filaments can subsequently reform by the drift of Al^{3+} ions from either electrode (depending on the polarity of the applied bias). There will be a dynamic equilibrium between filament formation and destruction, as first suggested by Dearnaley et al. [30, 31]. The voltage-controlled, 'N-shaped' current versus voltage characteristics (Figs. 2 and 3) results from non-regenerative filament formation, i.e. the resistance of the device is only slightly perturbed by the creation of a filament and the conditions are retained for the development of further filaments. The model also explains the (almost) Ohmic conductivity observed for the device ON state and is consistent with our observation that the switching process seems to be related to the electric field in the organic film. In previous work, we have suggested that the OFF state (in a formed device) is determined by conduction between the broken ends of the filaments [20]. However, the data revealed in this work suggest similar (within

experimental error) conduction processes in both the ON and OFF states. It is plausible that there is a residual network of (very fine) filaments when the device has switched OFF and that the conductivity of this provides the similar dependence of current upon voltage for both the ON and OFF states. The role of metallic nanoparticles is simply to provide nodes within the organic thin film where filaments can terminate and, importantly, sites where the redox processes involved in the filament growth can occur. Such effects stabilize the network of filaments, providing more reproducible electrical characteristics.

Some authors have suggested that the filament formation in resistive memory devices such as those described here occurs in the oxide layer(s) associated with the aluminium electrodes; when the filaments have broken down under the applied bias, the organic film merely acts as a current-limiting series resistance [32, 33]. Such an hypothesis is attractive, but the filamentary model presented here seems to provide a more complete explanation for all the experimental data. For example, according to our model, the device formation process will depend on the redox properties of the organic film and electrodes, and on the ability of the organic layer to transport metal ions. This explains why some metal/thin film/metal structures reported in the literature show no switching, while, in others 'S-shaped' (current-controlled) rather than 'N-shaped' (voltage controlled) NDR is observed. It also accounts for our earlier observation that switching and NDR do not occur if the molecular structure of the organic thin film is altered [19]. Experiments reported by Sebastian et al. [33] using a variety of organic semiconductors and different electrode materials reach a similar broad conclusion to ourselves (although the details of the filament formation process differ), i.e. that the charge transport in the device ON state is provided by the formation of localized channels within the organic material.

The model above can now be used to account for the results of our experiments with different electrode materials. The addition of an electron-blocking layer such as PEDOT:PSS on the bottom electrode essentially stops the device formation process by preventing the reduction of Al^{3+} ions (diffusing from the top electrode) to metallic aluminium. The current versus voltage characteristics are then determined by the nature (band structure and carrier mobilities) of the organic film and work

function of the electrodes. For the Al/PEDOT:PSS/organic film/Al structures studied in this work, this mechanism seems to be bulk-limited and is possibly Poole-Frenkel conduction.

Replacing the bottom Al electrode with Au also eliminates the switching and NDR effects. The extended Ohmic conductivity region at low bias for the Au-based devices indicates filamentary conduction. We suggest that this is the result of penetration of Au filaments though the organic layer during top electrode deposition. These filaments would appear to be more stable than those resulting from the use of an Al cathode and, once formed, cannot be destroyed by increasing the voltage.

The use of ITO as an electrode, which is well known for its ability to inject holes into organic electroactive compounds, results in a device with asymmetrical current versus voltage behaviour. When this electrode is positively biased, a significant hole current flows into the organic material; this masks any current carried by metallic filaments. The increase in current is simply due to the improved alignment of the Fermi level of the ITO (work function ~ 4.8 eV compared to ~ 4.2 eV for Al) with the HOMO level of the ambipolar compound (~ 5.3 eV) [35], providing a plentiful supply of holes. However, if the ITO electrode is negatively biased, switching and NDR effects are again observed.

The effects observed on incorporating the CsF layer between the organic thin film and the top Al electrode are perhaps the most intriguing (and most difficult to explain). First, the devices still exhibit NDR and switching phenomena even when a thick (10 nm) CsF layer is used. If the filament model shown in Fig. 8 is correct, this suggests that Al^{3+} ions can be transported through relatively thick insulating films. This result is consistent with our previous experiments with Langmuir-Blodgett (LB) films in which we incorporated either two or four layers of arachidic acid between the active organic layer and the Al top electrode [18]. The higher ON currents and the lower ON voltages suggest that filament formation is easier in the CsF structures. If CsF is considered to act as a simple insulator, then its presence beneath the top electrode would be to enhance hole injection into the organic film when a positive bias is applied to the top electrode (i.e. by allowing the Al Fermi level to move with respect to the HOMO level of the ambipolar compound), thereby enhancing the oxidation of Al to Al^{3+}. A further effect could be the diffusion of caesium and fluorine into the organic thin film,

doping the materials and, again, influencing the redox processes needed for filament formation. A plausible explanation for the decreasing switching voltage with the increasing CsF film thickness is that the drift of Cs^+ ions through the film contributes to (or dominates) the filament formation process.

3.5 Pulse Operation and Memory Retention

We have also taken the opportunity to make a preliminary study of some key device parameters affecting practical operation: pulse operation and device degradation. Aluminium/ambipolar organic film/aluminium and aluminium/ambipolar organic film + 0.5 wt. % NPs/aluminium structures with 1.5 mm wide electrodes were used to investigate the pulse operation and memory retention of our devices, respectively.

For pulse operation, a custom bias sweep having *n* steps at voltages of 1 V (read), 8 V (erase), 1 V (read), 4 V (write) and 1 V (read) (i.e. *n* x 1 V, *n* x 8 V, *n* x 1 V, *n* x 4 V and *n* x 1 V), with each step having a delay of *d* seconds before the start of the measurement cycle, was programmed into our Keithley 2400 Sourcemeter. By varying the values of *n* and *d*, the length of the read, write and erase pulses could be changed. Note that the length of the measurement cycle for our sourcemeter was variable (due to auto-ranging of the current meter) so that the total width of each pulse was usually greater than the product of *n* and *d*. Each device was subjected to the forming process and a bias of 4 V for 5 s to ensure that it was in the ON state before the pulses were applied.

Fig 9(a) shows the result of a pulse operation experiment where $n = 5$ and $d = 1$ s i.e. long pulses. It is clear from this graph that a long 8 V pulse switches the device from the ON to the OFF state and a long 4 V pulse restores it to the ON state. Fig 9(b) shows the result of a pulse operation experiment where n = 1 and d = 0.1 s i.e. short pulses. In this case, a short 8 V pulse switches the device into the OFF state but a short 4 V pulse does not fully restore it to the ON state. It is possible that a short write pulse does not allow sufficient time for the metallic filaments to reform after they have been destroyed by the erase pulse.

To investigate memory retention, two devices were subjected to the forming process and then one to a bias of 4 V for 5 s (to switch it into the ON state) and the other to 8 V for 5 s (to switch it into the OFF state). A 1 V read bias was then used to measure the current through each device at various times over a period of ~2 weeks. Between measurements, the devices were stored in a vacuum environment. The results of this experiment are shown in Fig. 10. The current through the device in the ON state (filled squares) initially falls, over a period of ~2 days, by a factor of 30 before saturating at a level of ~$1x10^{-7}$ A, whereas the current through the device in the OFF state (filled circles) remains fairly constant at ~$3\text{-}5x10^{-9}$ A. Although the memory window is initially reduced, the ON and OFF states are retained over the period investigated here. We should also note that we observed a reduction in both the ON and OFF state currents as a result of the time delay between device fabrication and the formation process. This accounts for the lower current values noted in Fig. 9(b); the phenomenon is currently under further investigation.

The above section represents preliminary measurements and, clearly, more detailed studies are needed to assess the viability of basing a memory/switching technology on filamentary conduction. However, the results to date indicate that reasonable lifetimes and switching behavior can be achieved in unencapsulated devices.

4. Conclusion

Switching and memory characteristics of metal/thin organic film/metal architectures, in which the organic material is an ambipolar compound based on oxadiazole (electron transporting) and carbazole (hole transporting) chemical groups, have been investigated. Switching and negative differential resistance phenomena are observed in the case of devices for which both electrodes are aluminium. Improved device characteristics (higher ON currents and ON/OFF ratios, less noisy and more reproducible behaviour) can be achieved by the incorporation of metallic nanoparticles within the organic film, and, to some extent, by the addition of a thin layer of CsF beneath the top Al electrode. Both the switching and NDR effects can be eliminated by coating the bottom Al electrode with

PEDOT:PSS or by replacing it with Au. The use of ITO as a bottom electrode obscures the switching and NDR when this electrode is positively biased. We suggest that our observations can be explained by a model based on the formation and destruction of Al filaments within the ambipolar film. Although, excellent switching behaviour (e.g. Fig. 3) can be demonstrated for individual devices, much research is needed to establish if reliable and reproducible memory arrays can ever be based on filamentary switching.

Acknowledgements

The authors would like to express their thanks to Professor Martin Bryce and Dr Katharine Linton (Chemistry Department, Durham University) for providing the ambipolar organic compound used in this work). MWL would also like to thank the School of Engineering and Computing Sciences at Durham University for hosting his visit to the UK.

References

[1] Petty M C 2007*Molecular Electronics: From Principles to Practice* (Wiley, Chichester)

[2] Sun S –J and Dalton L R (eds) 2008 *Introduction to Organic and Optoelectronic Materials and Devices* (CRC Press. Boca Raton)

[3] Cuevas J C and Scheer E 2010 *Molecular Electronics: An Introduction to Theory and Experiment* (World Scientific, Singapore)

[4] Klauk H (ed) 2012 *Organic Electronics II: More Materials and Applications* (Wiley-VCH)

[5] Claverie A, Tsoukalas D, King T –J and Slaughter J M (eds) 2005 *Materials and Processes for Nonvolatile Memories*, MRS Symposium Proceedings Volume 830 (Materials Research Society, Warrendale)

[6] Ling Q –D, Liaw D J, Zhu C, Chan D S –H, Kang E –T and Neoh K –G 2008 *Prog. Polym. Sci*. **33** 917-978

[7] *International Technology Roadmap for Semiconductors* 2012 URL http://www.itrs.net/reports.html [accessed July 31, 2013]

[8] Heremans P, Gelinck G H, Müller R, Baeg K –J, Kim D –Y and Noh Y –Y 2011 *Chem. Mater.* **23** 341-358

[9] Pershin Y V and Di Ventra M 2011 *Adv. Phys.* **60** 145-227

[10] Petty MC 2013 *Handbook of Organic Materials for Optical and Optoelectronic Devices*, ed O Ostroverkhova (Woodhead, Oxford) p 618

[11] Scott J C and Bozano L D 2007 *Adv. Mater.* **19** 1452-1463

[12] Cho B, Song S, Ji Y, Kim T –W and Lee T 2011 *Adv. Funct. Mater.* **21** 2806-2829

[13] Kim T W, Yang Y, Li F and Kwan W L 2012 *NPG Asia Materials* **4** e18, doi:10.1038/am.2012.32

[14] Strukov D B, Kohlstedt H 2012 *MRS Bulletin* **37** 108-114

[15] Lee T and Chen Y 2012 *MRS Bulletin* **37** 144-149

[16] Song S, Cho B, Kim T –W, Ji Y, Jo M, Wanf G, Choe M, Kahng Y H, Hwang H and Lee T 2010 *Adv. Mater.* **22** 5048-5052

[17] Lai Y-C, Wang Y-X, Huang Y-C, Lin T-Y, Hsieh Y-P, Yang Y-J and Chen Y-F 2013 *Adv. Funct. Mater.* DOI: 10.1002/adfm.201302246.

[18] Dimitrakis P, Normand P, Tsoukalas D, Pearson C, Ahn J H, Mabrook M F, Zeze D A, Petty M C, Kamtekar K T, Wang C, Bryce M R and Green M 2008 *J. Appl. Phys*. **104**, 044510

[19] Pearson C, Ahn J H, Mabrook M F, Zeze D A, Petty M C, Kamtekar K T, Wang C, Bryce M R, Dimitrakis P and Tsoukalas D 2007 *Appl. Phys. Lett*. **91** 123506

[20] Pearson C, Bowen L, Lee M –W, Fisher A L, Linton K E, Bryce M R and Petty M C 2013 Appl. Phys. Lett. **102** 213301

[21] Fisher A L, Linton K E, Kamtekar K T, Pearson C, Bryce M R and Petty M C 2011 *Chem. Mater*. **23** 1640–1642

[22] Bozano L D, Kean B W, Beinhoff M, Carther K R, Rice P M and Scott J C 2005 *Adv. Funct. Mater.* **15** 1933-1939

[23] Yang Y, Ouyang J, Ma L, Tseng R J-H and Chu C-W 2006 *Adv. Funct. Mater.* **16** 1001-1014

[24] Roberts G G, Apsley N and Munn R W 1980 *Physics Reports* **60** 59-150

[25] Hill R M 1971 *Phil. Mag.* **23** 59-86

[26] Joo W –J, Choi T –L, Lee J, Lee S K, Jung M –S, Kim N and Kim J M 2006 *J. Phys. Chem.* B **110** 23812-23816

[27] Wang Z S, Zeng F, Yang J, Chen C, Yang Y C and Pan F 2010 *Appl. Phys. Lett.* **97** 253301

[28] Mukherjee B, Ray A K, Sharma A K, Cook M J and Chambrier I 2008 *Appl. Phys. Lett.* **103** 074507

[29] Cho B, Jun J –M, Song S, Ji Y, Kim D –Y and Lee T 2011 *Adv. Funct. Mater*. **21** 3976-3981

[30] Dearnaley G, Morgan D V and Stoneham A M 1970 *J. Non-Cryst. Solids* **4** 593-612

[31] Dearnaley G, Stoneham A M and Morgan D V 1970 *Rep. Prog. Phys*. **33** 1129-1191

[32] Cölle M, Büchel M and De Leeuw D M 2006 *Organic Electronics* **7** 305-312

[33] Verbakel F, Meskers S C J, Janseen R A J, Gomes H L, Cölle M, Büchel M and De Leeuw D M 2007 *Appl. Phys. Lett*. **91** 192103

[34] Sebastian P, Lindner F, Walzer K and Leo K 2011 *J. Appl. Phys.* **110** 084508

[35] Linton K E, Fisher A L, Pearson C, Fox M A , Pålsson L-O, Bryce M R and Petty M C 2012 *J. Mater. Chem*. **22**, 11816–11825

Figures and Tables

Fig 1: Schematic diagram (a) and photograph (b) of the device structure; the molecular structure of the ambipolar molecule is shown in (c).

Fig 2: Current versus voltage characteristics for aluminium/ambipolar organic film/aluminium structures in which the organic layer was deposited at different spin speeds. The voltage scans for the different devices started at 0 V; the arrows indicate the scan directions.

Fig 3: Current versus voltage characteristics for aluminium/ambipolar organic film + 0.5 wt. % NPs/aluminium structures. The two sets of characteristics shown (indicated by the two different sets of symbols) correspond to consecutive measurements, both following the application of a voltage pulse with an amplitude close to the voltage minimum in the NDR region (8 V) to set the device in its OFF state. The voltage scans started at 0 V; the arrows indicate the scan directions. The inset shows the same data plotted as log(I) versus log(V).

Fig 4: (a) Current versus voltage characteristics for aluminium/PEDOT:PSS/ambipolar organic film/aluminium structures. Data sets shown for devices with and without NPs. (b) Data plotted in the form log(I/V) versus $V^{1/2}$. The voltage scans for the different devices started at 0 V; the arrows indicate the scan directions.

Fig 5: (a) Current versus voltage characteristics for ITO/ambipolar organic film/aluminium structures. (b) Data for negative bias (applied to Al electrode) in the form of log(I)

versus log(V). The voltage scans started at 0 V; the arrows indicate the scan directions.

Fig 6: Current versus voltage characteristics for gold/ambipolar organic film/aluminium structures. The insets show the data plotted in the form of log(I) versus log(V). The voltage scans started at 0 V; the arrows indicate the scan directions (positive direction first).

Fig 7: Current versus voltage characteristics for aluminium/ambipolar organic film/CsF/aluminium structures. Data for different thickness CsF films are shown. The voltage scans for the different devices started at 0 V; the arrows indicate the scan directions.

Fig 8: Model for filament formation.

Fig 9: Pulse operation of aluminium/ambipolar organic film/aluminium structures where (a) n, the number of steps at each bias level 1 V (read), 8 V (erase), 1 V (read), 4 V (write) and 1 V (read) = 5 and d, the measurement delay = 1 s and (b) n = 1 and d = 0.1 s. Bias, filled triangles; current filled circles.

Fig 10: Memory retention of aluminium/ambipolar organic film + 0.5 wt. % NPs/aluminium structures over a period of ~2 weeks using a read bias of 1 V. ON state device, filled squares; OFF state device, filled circles.

Table 1: Film thickness and average surface roughness (R_a) of ambipolar organic films deposited at different spin-coating speeds. Data are given for films before and after thermal annealing.

Table 2: ON/OFF ratio for device architectures with and without annealing (before Al top contact deposition) and with/without nanoparticles. Organic layer spin-coated at 700 rpm.

Table 3: ON voltage and ON/OFF ratio for aluminium/ambipolar organic film/CsF/aluminium structures; data are given for different CsF film thicknesses.

Table 4: Experimental observations for the switching behaviour for the various device architectures studied.

Spin speed [rpm]		500	700	1000
Unannealed	Film thickness [nm]	105	68	49
	Arithmetic average roughness R_a [nm]	0.36	0.34	0.37
Annealed	Film thickness [nm]	49	45	29
	Arithmetic average roughness R_a [nm]	0.34	0.33	0.41

Table 1

	ON/OFF ratio measured at 1 V
No annealing	
Without NPs	119.5
With NPs	288.1
With annealing	
Without NPs	3.9
With NPs	8.1

Table 2

CsF thickness [nm]	ON Voltage [V]	ON/OFF ratio measured at 1 V
0	3.5	500
0.6	3.0	1250
1.5	2.4	375
10	2.2	533

Table 3

Device Configuration	Observation
Al/organic/Al	Device formation is required to observe NDR and switching. Symmetrical I versus V characteristics. NPs generally increase current levels and give more reliable switching. ON voltage increases with ambipolar organic film thickness. ON/OFF ratio is thickness dependent. ON and OFF currents show $I \propto V^n$ with $n \sim 1.3$. Optimum organic layer thickness ~ 70 nm
Al/PEDOT:PSS/organic/Al	No switching or NDR for either bias polarity. Electrical characteristics suggest Poole-Frenkel conductivity.
Au/organic/Al	No switching or NDR. Symmetrical I versus V characteristics. $I \propto V$ for both polarities of bias up to 7 V.
ITO/organic/Al	Device forms with +ve voltage to top Al.No switching or NDR with –ve voltage to Al. For reverse bias, $I \propto V$ up to 10 V.
ITO/PEDOT:PSS/organic/Al	No switching or NDR.
Al/organic/CsF/Al	Devices reveal switching and NDR. ON voltage decreases with increasing CsF thickness. ON/OFF ratio is a maximum for CsF thickness of ~ 0.6 nm.

Table 4

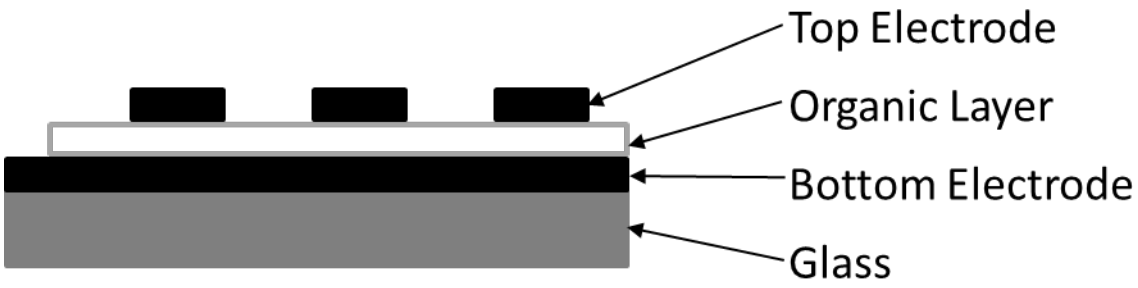
Top Electrode
Organic Layer
Bottom Electrode
Glass

(a)

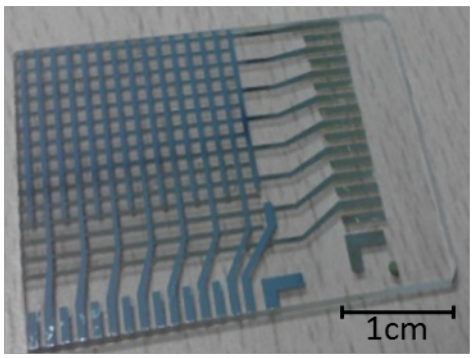
1cm

(b)

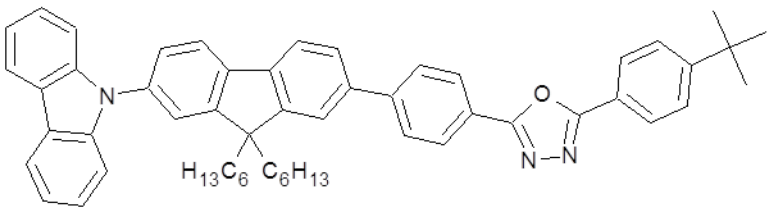
N
O
N
N
H13C6
C6H13

(c)

Fig 1

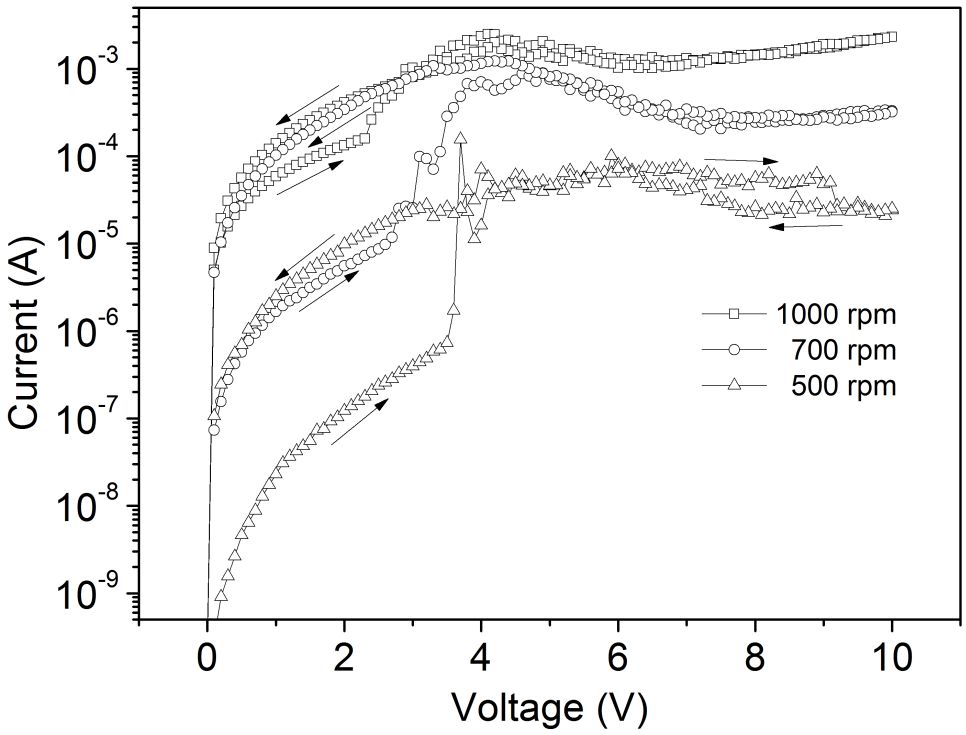
Current (A)
10-3
10-4
10-5
10-6
10-7
10-8
10-9
0
2
4
6
8
10
Voltage (V)
1000 rpm
700 rpm
500 rpm

Fig 2

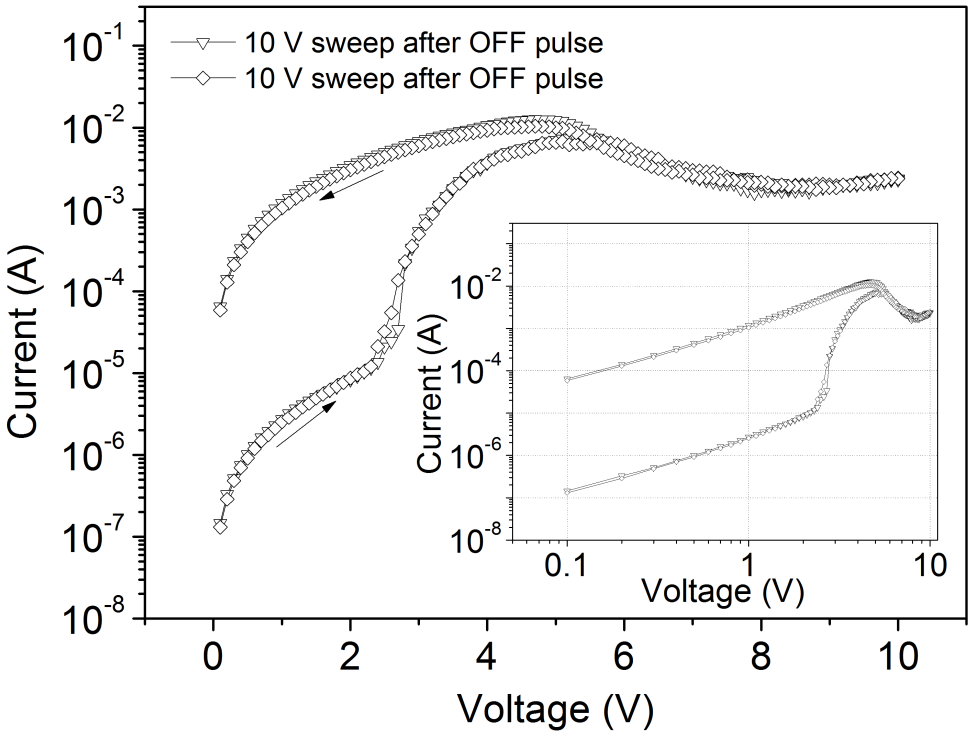
10 V sweep after OFF pulse
10 V sweep after OFF pulse
Current (A)
Voltage (V)
Current (A)
Voltage (V)

Fig 3

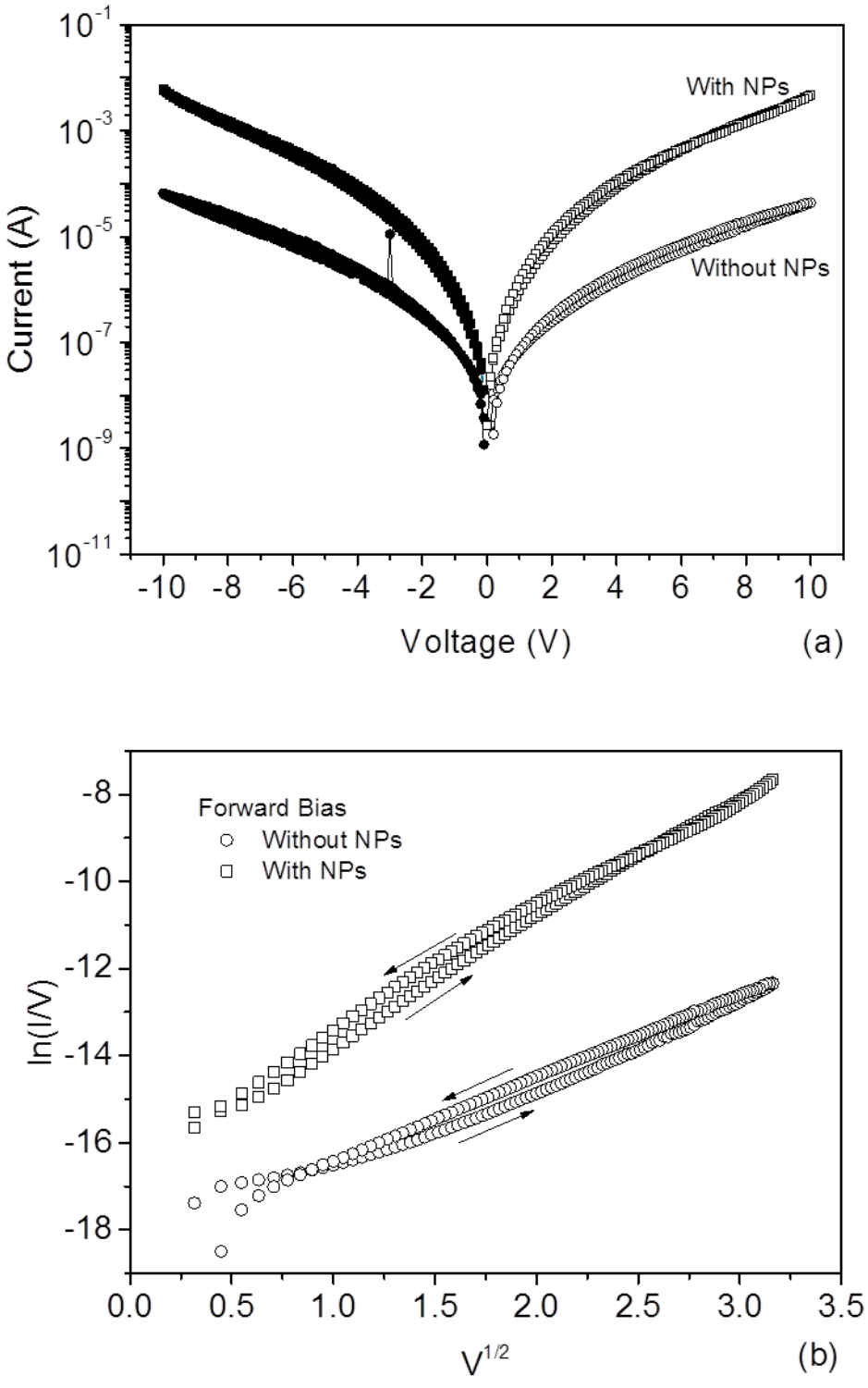
Current (A)
10^-1
10^-3
10^-5
10^-7
10^-9
10^-11
With NPs
Without NPs
-10 -8 -6 -4 -2 0 2 4 6 8 10
Voltage (V)
(a)
ln(I/V)
-8
-10
-12
-14
-16
-18
Forward Bias
Without NPs
With NPs
0.0 0.5 1.0 1.5 2.0 2.5 3.0 3.5
V^1/2
(b)

Fig 4

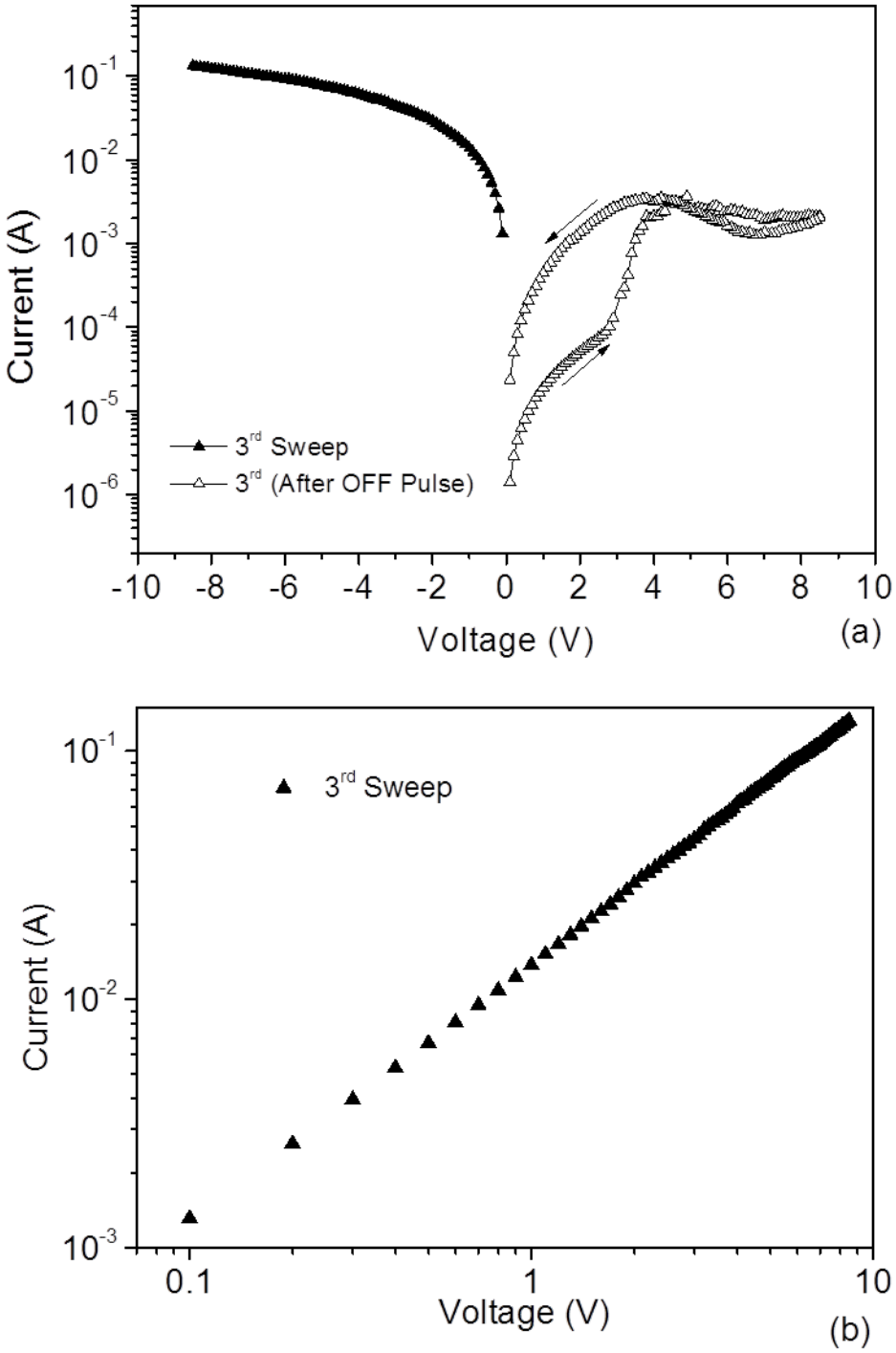
Current (A)
10^{-1}
10^{-2}
10^{-3}
10^{-4}
10^{-5}
10^{-6}
3rd Sweep
3rd (After OFF Pulse)
-10 -8 -6 -4 -2 0 2 4 6 8 10
Voltage (V)
(a)
Current (A)
10^{-1}
10^{-2}
10^{-3}
3rd Sweep
0.1
1
10
Voltage (V)
(b)

Fig 5

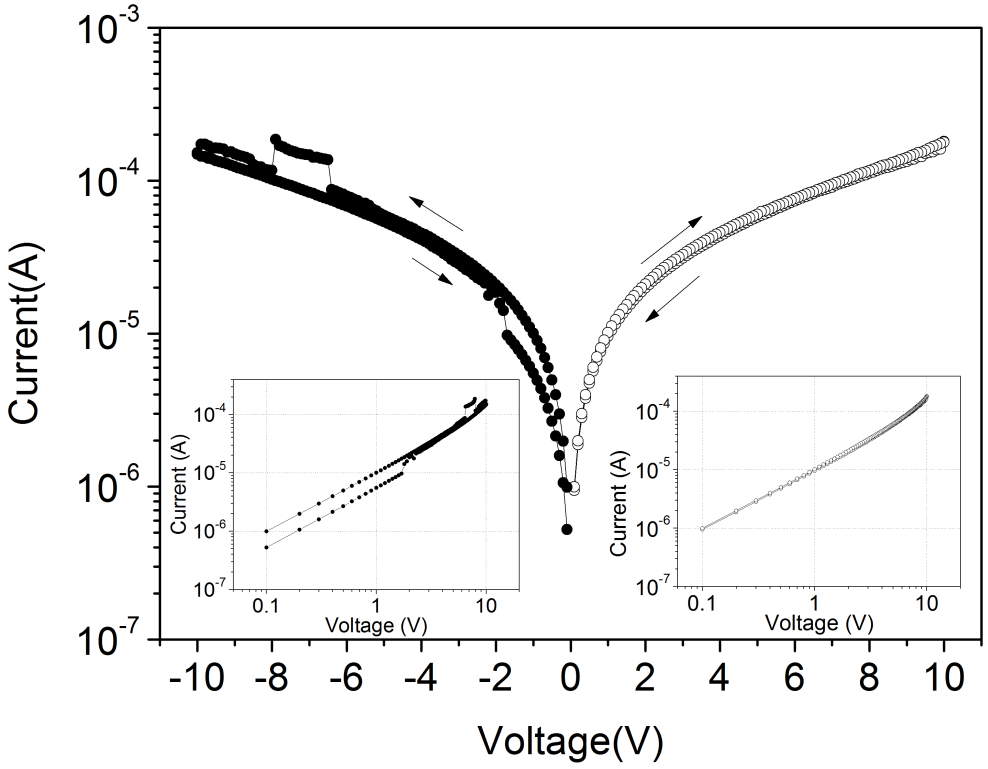

Fig 6

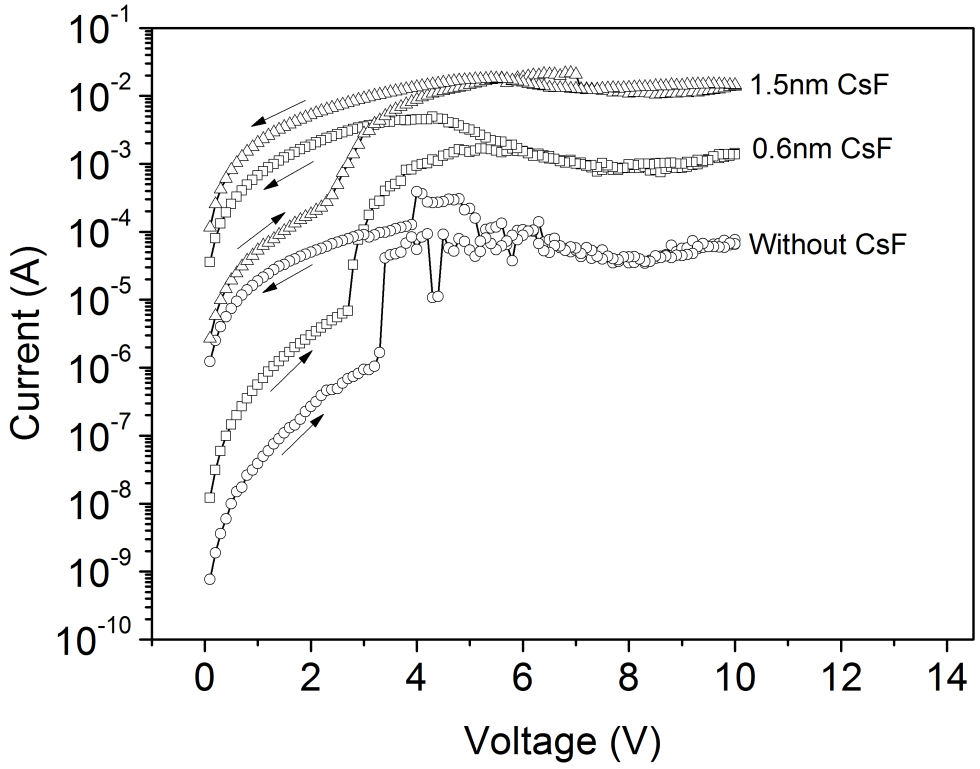
Current (A)
Voltage (V)
1.5nm CsF
0.6nm CsF
Without CsF
10^-1
10^-2
10^-3
10^-4
10^-5
10^-6
10^-7
10^-8
10^-9
10^-10
0
2
4
6
8
10
12
14

Fig 7

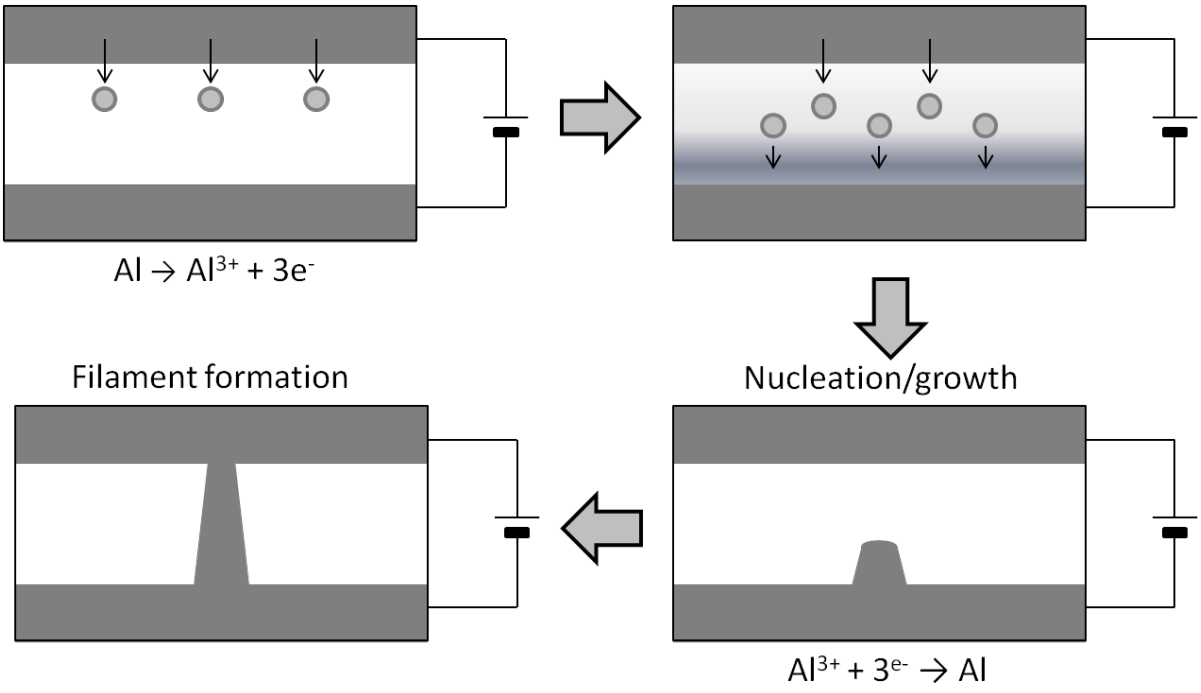

Fig 8

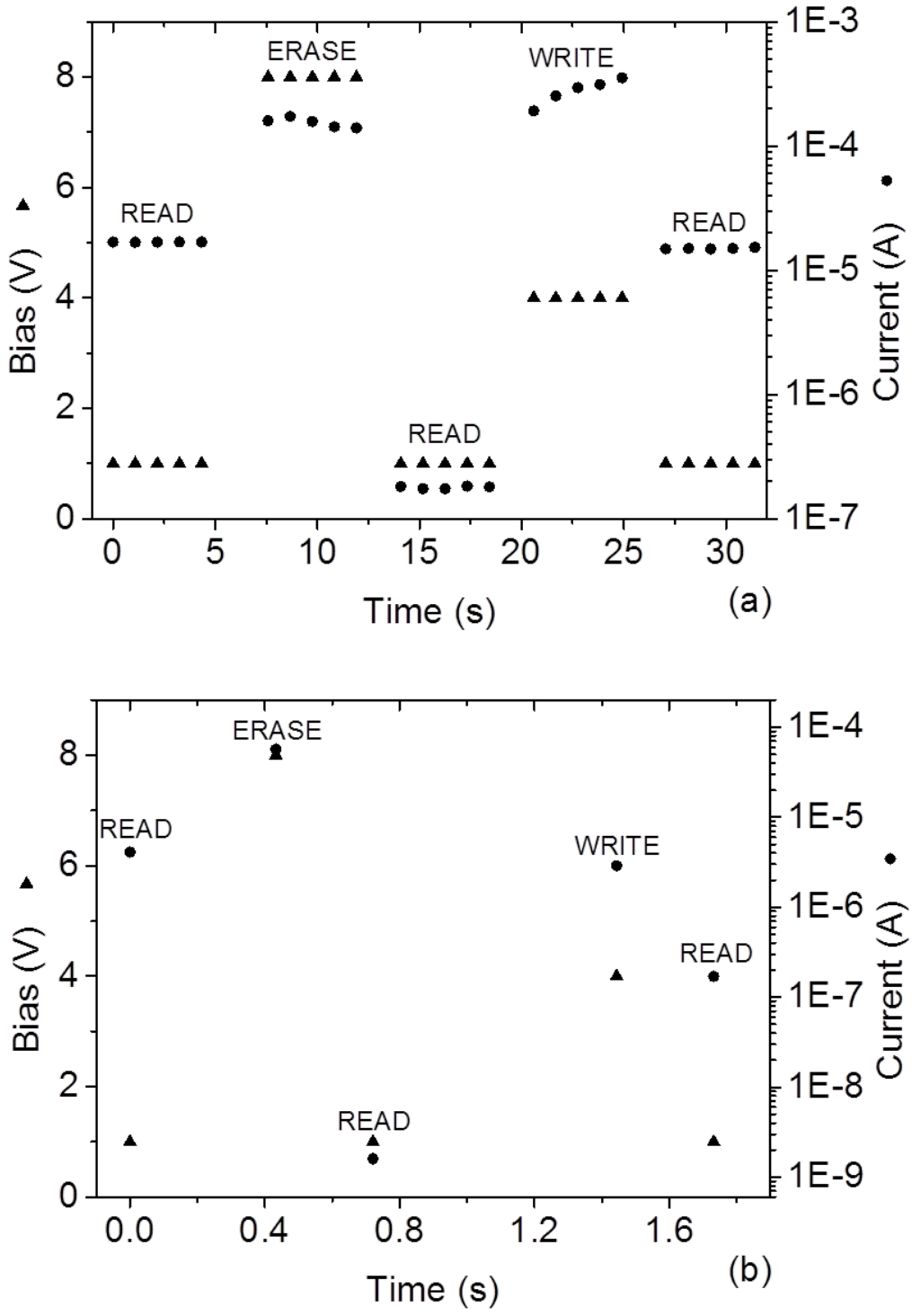
ERASE
WRITE
READ
READ
READ
Bias (V)
Current (A)
Time (s)
(a)
ERASE
READ
WRITE
READ
READ
Bias (V)
Current (A)
Time (s)
(b)

Fig 9

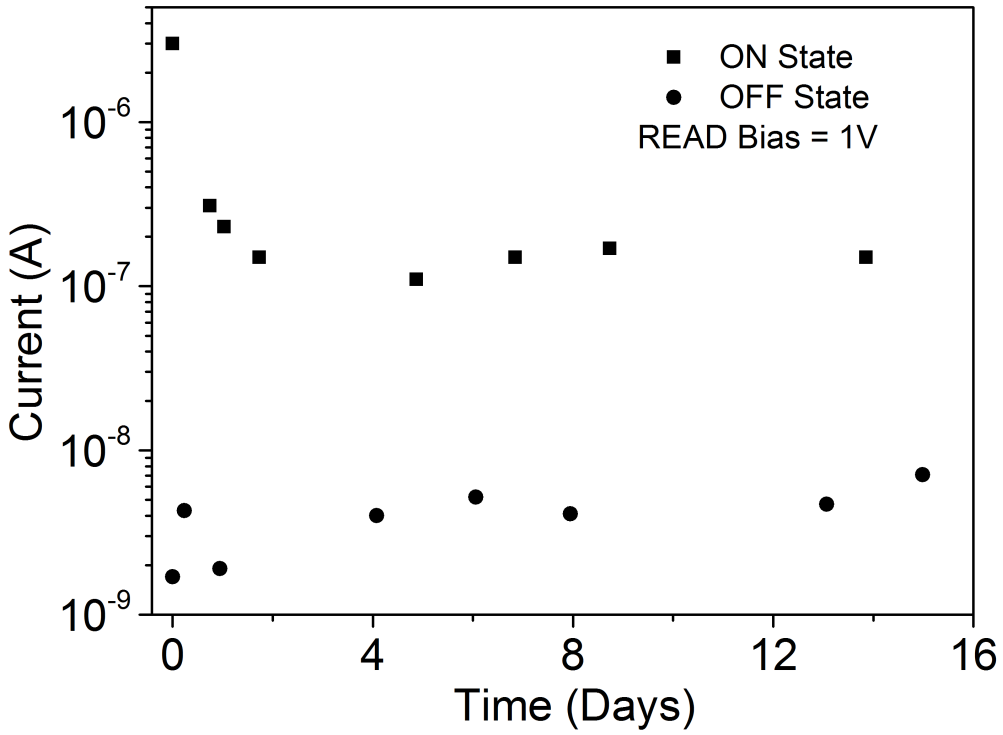
ON State
OFF State
READ Bias = 1V
Current (A)
10-6
10-7
10-8
10-9
0
4
8
12
16
Time (Days)

Fig 10